Journal of Ovonic Research Vol. 9, No. 2, March - April 2013, p. 61 - 71

INVESTIGATION OF BORON AND YTTRIUM DOPING EFFECT ON STRUCTURAL, ELECTRICAL AND OPTICAL PROPERTIES OF SOL-GEL SPIN COATED SnO_2 THIN FILMS

E.F. KESKENLER[a*], G. TURGUT[b], S. AYDIN[b], R. DILBER[b], U. TURGUT[b]
[a]*Recep Tayyip Erdoğan University, Faculty of Arts and Sciences, Department of Physics, 53100 Rize, Turkey*
[b] *Ataturk University, K.K. Education Faculty, Department of Physics, 25240 Erzurum, Turkey*

In this study, B and Y doped SnO_2 thin films were prepared by sol-gel spin coating method. The structural, electrical and optical properties of doped SnO_2 were investigated as a function of B and Y doping content. From XRD analysis, it was seen that the films had hetero-phase structure with cubic, orthorhombic, tetragonal and (111) cubic phase was the most striking phase for B and Y doped films, except for 7 at. % Y doped SnO_2 films. It was seen from electrical measurement that sheet resistance values increased with B and Y doping content. The optical properties of films were extensively investigated as a function of B and Y doping content. And it was found that the optical transmittance, reflectance, extinction coefficient, refractive index, band gap and Urbach energy values depended on B and Y doping concentration. Also, it was observed that B doped films had the better structural, electrical and optical properties than Y doped films.

(Received February 7, 2013; Accepted April 4, 2013)

Keywords: B and Y doping; SnO_2; Sol-gel; Hetero-phase; Urbach rule.

1. Introduction

SnO_2 is used widely in many fields owing to its high optical transparency and electrical conductivity, superior chemical stability, low cost [1,2], high infrared reflectivity [3-6]. The stoichiometric SnO_2 is a good insulator, but non-stoichiometry makes it n-type semiconductor due to intrinsic defects [7-10] (oxygen vacancies or tin interstitials). The doping of the SnO_2 films could be achieved by replacing Sn^{4+} and O^{2-} atoms with dopant atoms. The efficiency of dopant atoms depend on difference between their ionic radius and ionic radius of host atoms (tin or oxygen) [10]. Theoretically, effective substitution of Sn^{4+} and O^{2-} by X^{m+} (m>4) and Z^{-} elements increase the n-type conductivity [7,11,12], but the substitutions of Sn^{4+} by Y^{n+} (n<4) elements can decrease n-type conductivity and can make p-type conductivity [2,13-14] which would trap free electrons leading to the reduce of free electrons. In present study, for SnO_2 structure, the elements of boron (B) and yttrium (Y) with +3 oxidation states have been used as dopant atoms. B and Y separately doped SnO_2 thin films have been synthesized via sol-gel spin coating technique. In earlier studies, B and Y doped SnO_2 structures have been prepared by spray pyrolysis [15,16], polymeric precursor method [17], (RF) reactive ion-beam sputtering [18]. However, to the best our knowledge, the fabrication of both B and Y separately doped SnO_2 thin films have not been reported up to now by sol-gel spin coating method. Therefore, in this study, we intend to investigate the effect of B and Y doping on structural, electrical and optical properties of SnO_2 thin films prepared by sol-gel spin coating method. The sol-gel spin coating technique is attractive due to its easy manipulation of the samples, ability to prepare high quality thin films in large scale,

* Corresponding author: keskenler@gmail.com

simplicity, safety, low cost of apparatus [19], deposition of high purity, homogeneous, cheaper, large-area films at relatively low temperatures [20,21], easy control of chemical components [22].

2. Experimental

In the present study, B and Y doped tin oxide thin films were prepared by sol-gel spin coating method on glass substrates. The coating precursor solutions was prepared by using stannous chloride dihydrate ($SnCl_2.2H_2O$) as a starting material. 2- methoxyethanol ($C_3H_8O_2$) and monoethanolamine (C_2H_7NO, MEA) were used as solvent and stabilizer, respectively. The molar ratios of $SnCl_2.2H_2O$ and metal dopant sources to MEA were maintained at 1:1. For the B and Y doped doped samples respectively, 0.1 M trimethyl borate ($B(OCH_3)_3$) and 0.1 M yttrium(III) chloride (YCl_3) were mixed separately in different solutions to obtain the mole ratios as 1, 3 5 and 7 at. %. The precursor sols were stirred at 60 ^oC for 10 h in a tightly-closed flask to obtain a clear and homogenous solution. The glass substrates the firstly were kept in boiling chromic acid solution and then they were rinsed with deionized water. Finally, they were cleaned with acetone, methanol and deionized water by using an ultrasonic cleaner and dried with nitrogen. The resultant solutions being dropped on glass substrates were rotated at a speed of 2500 rpm for 25 sec by using a spin-coater. After the glass substrates were coated, they were sintered at 200 ^oC for 5 min to evaporate solvent and remove the organic sediments and then spontaneously cooled to room temperature. This procedure was repeated for 10 times and finally, the samples were annealed in air at 450 ^oC for 30 minutes.

The structural characterization of the B and Y doped thin films was carried out by X-ray diffraction (XRD) measurements using a Rigaku Miniflex II diffractometer with CuKα radiation (λ=1.5418 Å). The diffractometer reflections were taken at room temperature and the values of 2θ were altered between 10^o and 70^o. The optical transmittance of the samples was recorded in spectral region of 300-1000 nm at 300 K using a UV-VIS spectrophotometer (Perkin-Elmer, Lambda 40) which works in the range of 200-1100 nm. The sheet resistance values of films were measured by means of four point probe technique.

3. Results and discussions

3.1. Structural properties

The crystal structure of samples has investigated by X-ray diffraction (XRD) patterns. Fig. 1 (a-b) shows XRD spectra of B and Y doped SnO_2 thin films, respectively. As seen from these spectra, B doped at all content and 1, 3, 5 at. % Y doped samples are grown at (111) preferential orientation corresponding to SnO_2 cubic phase (JCPDS 50-1429), but 7 at. % Y doped sample is grown orthorhombic (110) orientation (JCPDS card no:29-1484). The orthorhombic (110) peak are observed slightly for other samples, also the planes of (110), (101) corresponding to SnO_2 tetragonal rutile phase (JCPDS 41-1445) is seen at very low intensities. No additional peaks which imply oxides of yttrium and boron are not observed. In general, SnO_2 crystallize in the tetragonal rutile crystal system, but there are also orthorhombic and cubic phases of SnO_2. The cubic phase of SnO_2 has observed by Shien [23], Haines and Legér [24] under high pressure. In recent years, cubic, orthorhombic and tetragonal phases (separately or hetero-pahase structure) have been reported from the experiments studies based on the solutions performed at atmospheric pressure [25-27]. In this study, SnO_2 hetero-phase structure has been obtained at atmospheric pressure. For both B and Y doped samples, the peaks intensities of undoped sample have decreased continuously with increasing doping contents. Moreover, the peak intensities of B doped samples are more than Y doped samples, which implies better crystalline of B doped films.
The inter planer ‘d’ values of the most striking peaks have calculated by Bragg’s law [28]

$$n\lambda=2d\sin\theta \quad (1)$$

where n is 1, λ is the wavelength of the incident X-ray beam which is 1,5418Å and θ is the diffraction angle. The calculated 'd' values are presented in Table 1 and these values are compared with the standard value from the JCPDS 50-1429, 41-1445, 29-1484 data files. The grain size values have calculated by Scherrer's Formula [29]

$$D = \frac{0,9\lambda}{\beta\cos\theta} \quad (2)$$

where D is the crystallite size, wavelength of the X-ray used is λ =1.5418 Å, β is the broadening of diffraction line measured at the half of its maximum intensity in radians and θ is the angle of diffraction. The variation of grain size and dislocation density values of Y and B doped SnO_2 films is given in Table1. As seen in Table1, for B doped samples, the grain size value of 79.08 nm for 1 at. % B doped sample is increased to 91.07 nm value for 3 at. % doping ratio. When the B doping ratio is 5 at. % , this value is decrease to 60.91 nm and then again increases to 62.85 nm value. For Y doped samples, the value of 68.44 nm for 1 at. % Y doped increases with Y doping content, but grain size value of 7 at. % Y doped sample is not measured due to its nearly amorphous phase.
The dislocation density(δ), defined as the length of dislocation lines per unit volume (lines /m^2) and the dislocation density (δ) is the measure of the amount of the defects in a crystal. The dislocation density values of films have calculated by relation [30]

$$\delta = 1/D^2 \quad (3)$$

The smallest dislocation density values films are calculated to be $1.20x10^{14}$ lines/m^2 and $1.58x10^{14}$ lines/m^2 for 3 at. % B and 5 at. % Y doping ratio, respectively.

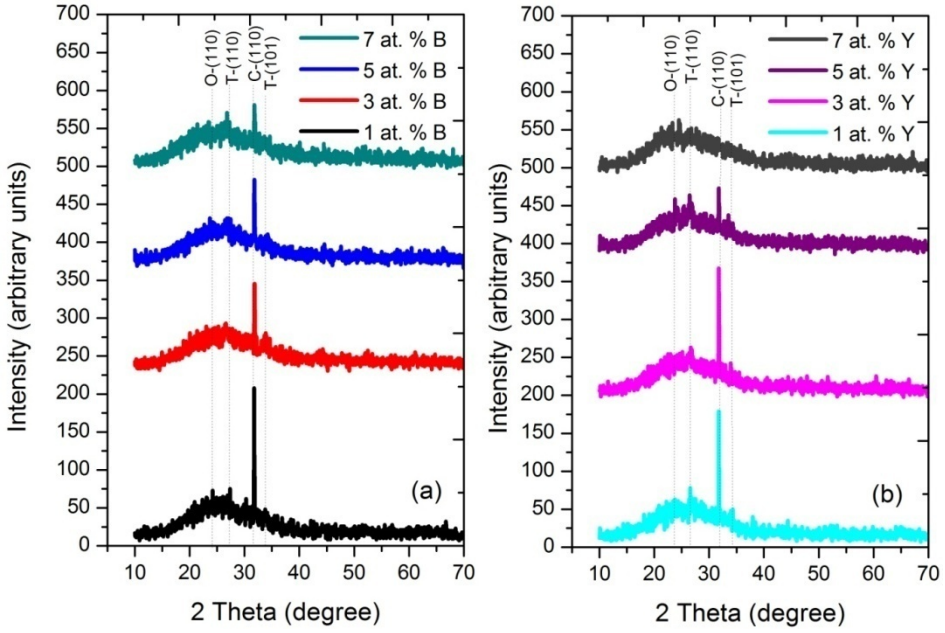

Fig. 1. XRD spectra of the films; (a) B doped SnO_2 (b) Y doped SnO_2 films

Table 1. The structural properties of B and Y doped SnO_2 films

Sample	(hkl)	2 theta (Degree)	d (A)	FWHM (Degree)	D (nm)	δ (x10^{14} lines/m^2)
1.0 at. % B doped	T-110	26.890	3.3128	0.150	79.08	1.60
	C-111	31.755	2.8156	0.102		
	T-101	33.755	2.6532	0.205		
3.0 at. % B doped	T-110	26.377	3.3761	0.271	91.47	1.20
	C-111	31.849	2.8074	0.089		
	T-110	33.935	2.3835	0.181		
5.0 at. % B doped	O-110	23.800	3.7354	0.102	60.91	2.70
	T-110	26.700	3.3360	0.364		
	C-111	31.802	2.8115	0.133		
	T-101	34.307	2.6117	0.293		
7.0 at. % B doped	O-110	23.417	3.7957	0.112	62.85	2.53
	T-110	26.711	2.3345	0.110		
	C-111	31.811	2.8107	0.129		
1.0 at. % Y doped	T-110	26.582	3.3506	0.186	68.44	2.13
	C-111	31.770	2.8143	0.118		
	T-101	34.335	2.6097	0.082		
3.0 at. % Y doped	T-110	26.624	3.3453	0.415	70.20	2.03
	C-111	31.764	2.8148	0.115		
	T-101	33.887	2.6431	0.110		
5.0 at. % Y doped	O-110	23.756	3.7423	0.146	79.88	1.58
	T-110	26.456	3.3663	0.050		
	C-111	31.758	2.8153	0.101		
	T-101	33.559	2.6682	0.128		
7.0 at. % Y doped	-	-	-	-	-	-
Standard d values	O-110	24.434	3.6400	JCPDS 28-1484		
	T-110	26.611	3.3470	JCPDS 41-1445		
	C-111	31.796	2.8120	JCPDS 50- 1429		
	T-101	33.893	2.6427	JCPDS 41-1445		

3.2. Electrical properties

The electrical properties of B and Y doped samples have measured by four point probe. The variation of sheet resistance with doping ratios is given in Fig. 2 and Table 2. As can be seen in Fig.2 and Table 2, sheet resistance value of 68.72 kΩ for 1 at. % B doped SnO_2 , the firstly decreases to 55.22 kΩ for 3 at. % B doping ratio and then increases to 93.28 and 352.8 kΩ values for 5 and 7 at. % B doping ratios, respectively. For Y doped samples, sheet resistance continuously increases from 104.8 kΩ to 1450 kΩ with increasing Y doping ratio. When SnO_2 is doped with B and Y, Sn^{4+} ions in lattice can replaced by B^{3+} and Y^{3+}, resulting in the formation of acceptor states and a concomitant loss of carriers and an increase at the sheet resistance [1-3,13,14]. Another reason for increasing sheet resistance of B and Y doped samples may be shown that B and Y atoms may not place proper lattice position with increasing doping ratios and resulting transition of an amorphous phase which may be caused by the high ionic radii of B and Y than Sn [16,31]. However, reason for decreasing sheet resistance 1 at. % B doping ratio, may be that the majority of B^{3+} ions cannot replaced with Sn^{4+} and the boron ions may occupy the interstitial sites and release three free electrons resulting in an increase of free electrons concentration [15]. Also, the sheet resistance values of B doped films are little than Y doped films. It can be caused by better

crystallinity of B doped films because, as seen from Fig 1, the peak intensities of B doped films more than Y doped films.

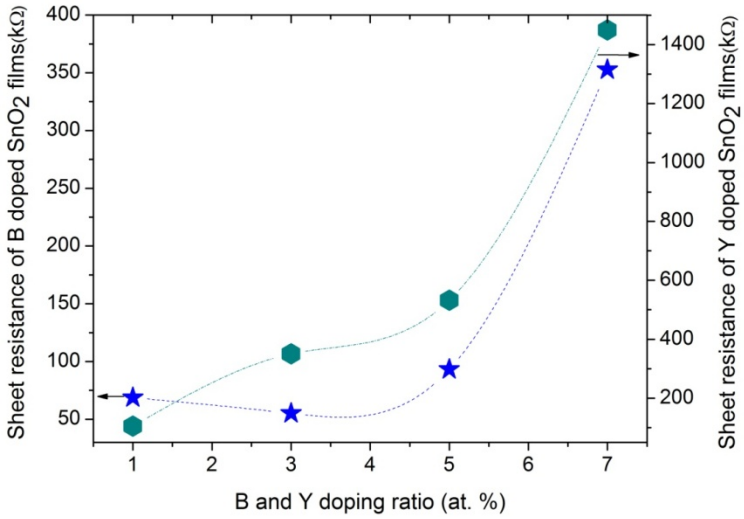

Fig. 2. The variation of sheet resistance of SnO_2 films with B and Y doping ratio

Table 2. Electrical and optical properties of B and Y doped SnO_2 films.

Sample	Rs (kΩ)	Transmittance values at various wavelength (%-T)				Eg (eV)	Eu (meV)	σ steppness
		at 550 nm	at 650 nm	at 750 nm	at 850 nm			
1 at. % B doped	68.72	71.10	71.58	72.18	72.67	4.02	128	0.202
3 at. % B doped	55.22	69.42	69.23	69.44	70.06	4.01	135	0.192
5 at. % B doped	93.28	66.58	67.18	67.56	68.17	3.99	144	0.179
7 at. % B doped	352.8	64.28	65.92	67.08	68.18	3.97	130	0.199
1 at. % Y doped	104. 8	67.66	67.92	68.69	69.43	4.01	148	0.175
3 at. % Y doped	350.3	67.73	68.59	69.01	69.75	4.00	136	0.190
5 at. % Y doped	532.4	69.77	69.33	69.15	69.01	3.98	145	0.178
7 at. % Y doped	1450	65.57	68.04	68.05	68.10	3.96	147	0.176

3.3. Optical properties

The optical properties of B and Y doped SnO_2 thin films were investigated by UV-VIS spectrometer at room temperature. The absorption and transmittance spectra are given in Fig 3 a-b-d-e. From transmittance spectra, 1 at. % B doped films exhibits transmittance values of 71.10 % , 71.58 %, 72.18 %, 72.67 % at 550, 650, 750 and 850 nm wavelength, respectively. When the B

doping concentration is increased, the transmittance values at these wavelengths change to 69.42 %, 69.23 %, 69.44 %, 70.06 %; 66.58 %, 67.18 %, 67.56 %, 68.17 %; 64.28 %, 65.92 %, 67.08 %, 68.18 % values, for 3; 5; 7 at. % B doped SnO_2 samples, respectively. For 1 at. % Y doped sample, the transmittance values of 67.66 %, 67.92 %, 68.69 %, 69.43 % at 550, 650, 750 and 850 nm wavelength, change to values of 67.73 %, 68.59 %, 69.01 %, 69.75 %; 69.77 %, 69.33 %, 69.15 %, 69.01 %; 65.57 %, 68.04 %, 68.05 %, 68.10 % for 3; 5; 7 at. % Y doped samples. As seen from these values, the transmittance values of all films increase at high wavelength, this can be resulted from decreasing reflectance of films. And for all films, the transmittance at short wavelength shifts red with increasing doping contents. At all doping ratio, the transmittance values of B doped samples are more than Y doped samples. This can be given rise to that the crystallinity of B doped films are better than Y doped films.

The reflectance (R) of the films is found by using relationship [32]

$$R+T+A=1 \quad (4)$$

where T and A were transmission and absorption. Reflectance (%) spectra of B and Y doped samples were given in Fig. 3c-e. These spectra show that the reflectance of films at short wavelength is high, and the values of R decrease as increasing wavelength. In this case, Drude's model can be used to study the decrease in reflectance and increase in transmittance in the near infrared region (NIR) [11]. According to this model, it is expected a increasing in transmittance in NIR region with decreasing carrier concentration. We can concluded from decreasing sheet resistance values with doping content, which Sn^{4+} ions in lattice is replaced by B^{3+} and Y^{3+}, resulting in the loss of carriers [13,14], except for 3 at. % B doped sample.

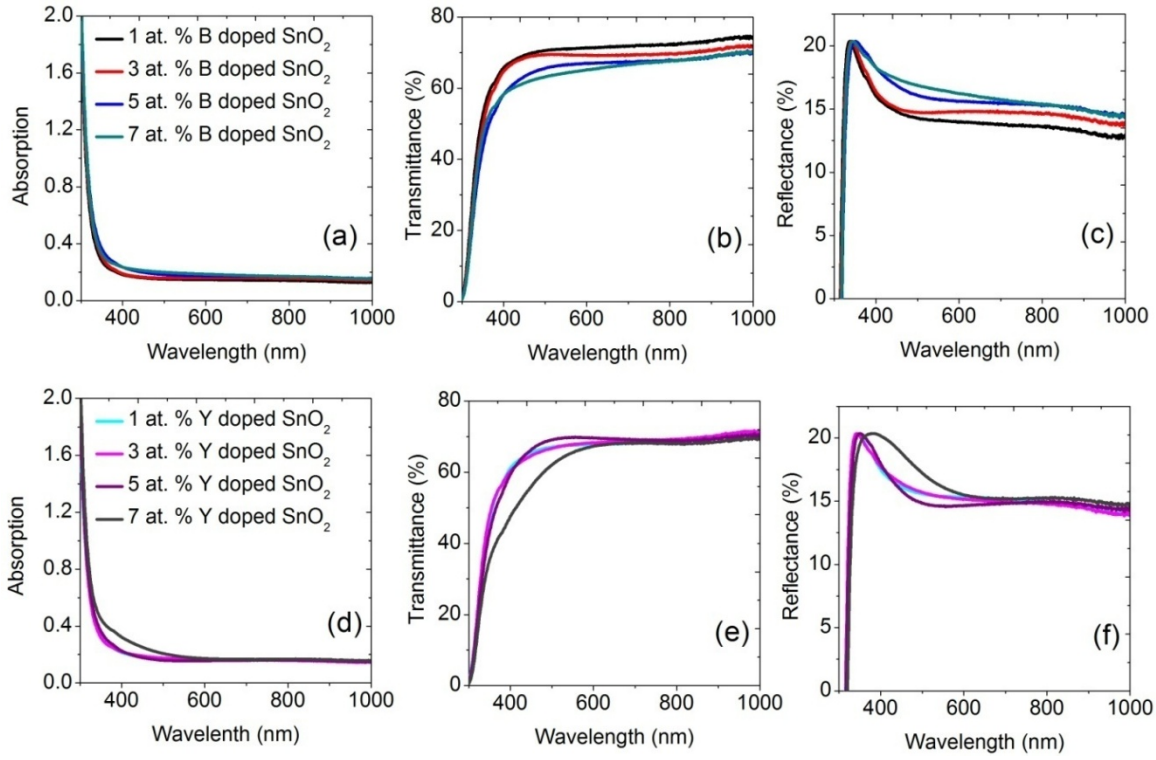

Fig. 3. The optical absorption, transmittance and reflectance spectra of B and Y doped films

Refractive index (n) of the samples and extinction coefficient (k) are calculated by relation [33]

$$n = \frac{1+R}{1-R} + \sqrt{\frac{4R}{(1-R)^2} - k^2} \quad (5)$$

and

$$k = \frac{\alpha\lambda}{4\pi} \quad (6)$$

where R is reflectance, α is absorsoption coefficient and λ is wavelength. The n and k values dependence on wavelength is shown in Fig 4 (a-d) for B and Y doped samples. From these figures, it can be seen that n and k values depend on wavelength. The extinction coefficient values of all films firstly have decreasing tendency with increasing wavelength up to 400 nm, and then increasing tendency with further increasing wavelength. Also, k values decrease with increasing doping content for both B and Y content. For 1, 3, 5 and 7 at. % B doped films, respectively; the average n values are 2.21, 2.26, 2.32, and 2.34. These values are 2.29, 2.30, 2.28, 2.34 for 1, 3, 5 and 7 at.% Y doped samples, respectively. The average refractive index values of all films are agreement with values of SnO_2 refractive index reported by other researchers [34-36] and this conclusion compare with other studies [37,38].

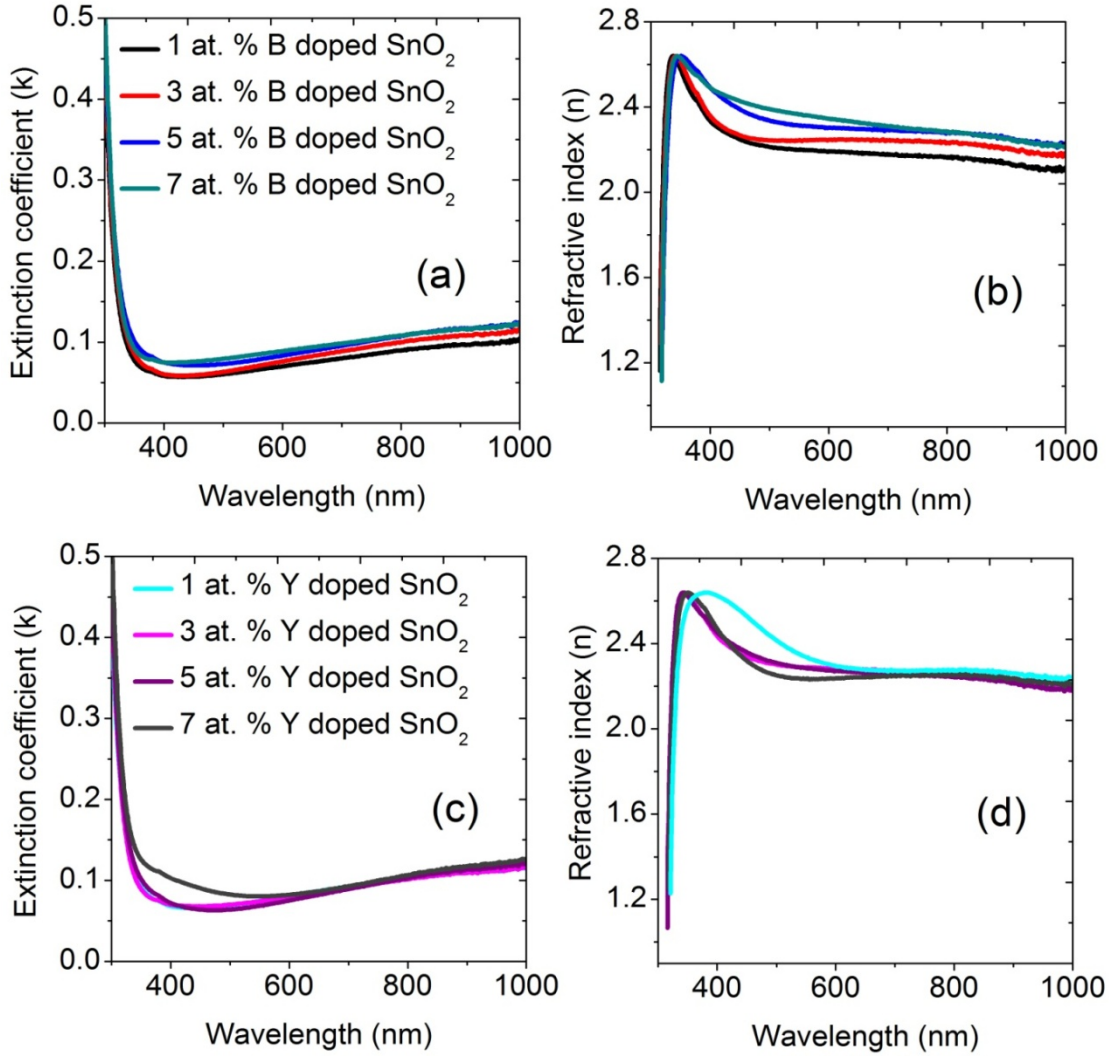

Fig. 4. The extinction and refractive index variation with wavelength of B and Y doped SnO_2 films

The absorption coefficient (α) of the films is determined by Lambert's equation [39],

$$\alpha = \ln (1/T)/d \tag{7}$$

where T is transmittance and d is film thickness. The optical band gap is obtained by following relation [40],

$$\alpha h\nu = A(h\nu - E_g)^{1/2} \tag{8}$$

according to the relationship equation (8), where hν and A were photon energy and the constant, respectively. The band gap (E_g) values of the films were determined by plotting $(\alpha h\nu)^2$ vs. hν and extrapolating of the linear region of the plot to zero absorption ($(\alpha h\nu)^2 = 0$) (in Fig.2). E_g values of 1, 3, 5 and 7 at. % B doped films were found as 4.02, 4.01, 3.99 and 3.97 eV, respectively. For Y doped films at 1, 3, 5, 7 atomic ratios %, they were found as 4.01, 4.00, 3.98 and 3.96 eV, respectively, Namely, band gap values of both B and Y doped films decrease slightly with increasing doping content. The reason for decreasing band gap with increasing doping content can explained as follows; SnO_2 is one of degenerate semiconductors [8], which the Fermi level lies within the conduction band. Thus, the optical band gaps are related to the excitation of the electrons from the valance band to Fermi level [11,41]. This means that the Fermi level going down to the bottom of conduction band of the degenerate semiconductor due to the decrease in the carrier density leads to the energy band narrowing with some of the Sn^{4+} ions in the lattice are replaced by $B^{3+}$and Y^{3+}. SnO_2 doped with 3 at. % B sample has the lowest sheet resistance, optical band gap value is lower 1 at. % B doped sample and this is contradictory with the above explanations, but this may be caused from reduction in crystallinity and increase in the structural disorders.

The absorption edge is sensitive to temperature and disorder in the film which leads to broadening of the absorption edge. The density of states is not actually zero at the band gap of the material. A formation occurs in the band tails named Urbach tails which are tails of band state densities extending into the band gap [42]. The disorder causing increase to exponential band tails is produced by the impurities, lattice vibrations and other actions from the lattice. The optic transition between band to tail is effective on the exponential rise of the absorption coefficient at the absorption edge, which is expressed by the Urbach [43].

An exponential increasing in the absorption edge in a number of materials that including ionic crystals, semiconductors, and organic crystals follows the empirical formula that Urbach energy is given below [43]:

$$\alpha = \alpha_0 exp\left(\frac{h\nu - E_0}{E_U}\right) \tag{9}$$

where E_0 and α_0 are characteristic parameters of the material and E_U is the Urbach energy which refers to the width of the exponential absorption edge. The Urbach energy (E_U) was calculated from the variation of lnα versus photon energy and given in Table 2. Addition to the thermal component effect to the structural disorder system, there is an additional non-thermal component effect to the disorders which impurities and defects in crystal structures [44]. Urbach energy values of the films fluctuate with B and Y doping. In generally, the optic band gaps of the samples change reversely with Urbach energy. This result causes a redistribution of states, such as from band to tail and tail to tail transitions [45] and in order, the optical gap decreases because of the broadening of the Urbach tail. It can be seen that B incorporation causes more changing in the Urbach energy values, than that of Y incorporation, as a result of rising disorder.

Eq. (9) can be rewritten as;

$$\alpha = \alpha_0 exp\left(\frac{\sigma(h\nu - E_0)}{k_B T}\right) \tag{10}$$

where σ is called steepness parameter, which characterizes the steepness of the straight line near the absorption edge because of the electron-phonon or exciton–phonon interaction [46], T is the temperature and k_B is the Boltzmann constant. If E_U is related to the slope absobtion edge and from Eq. (10), the σ parameter is calculated;

$$\sigma = k_B T / E_U \tag{11}$$

The σ values were calculated using equ. (11) for T = 300 K. The calculated values are given in Table 2. Fig. 5-b and -d show the hν vs. ln(α) for B and Y doped SnO_2 films for Urbach energy. As can be clearly seen from Table 2, the steepness parameters change reversely as the Urbach energy values.

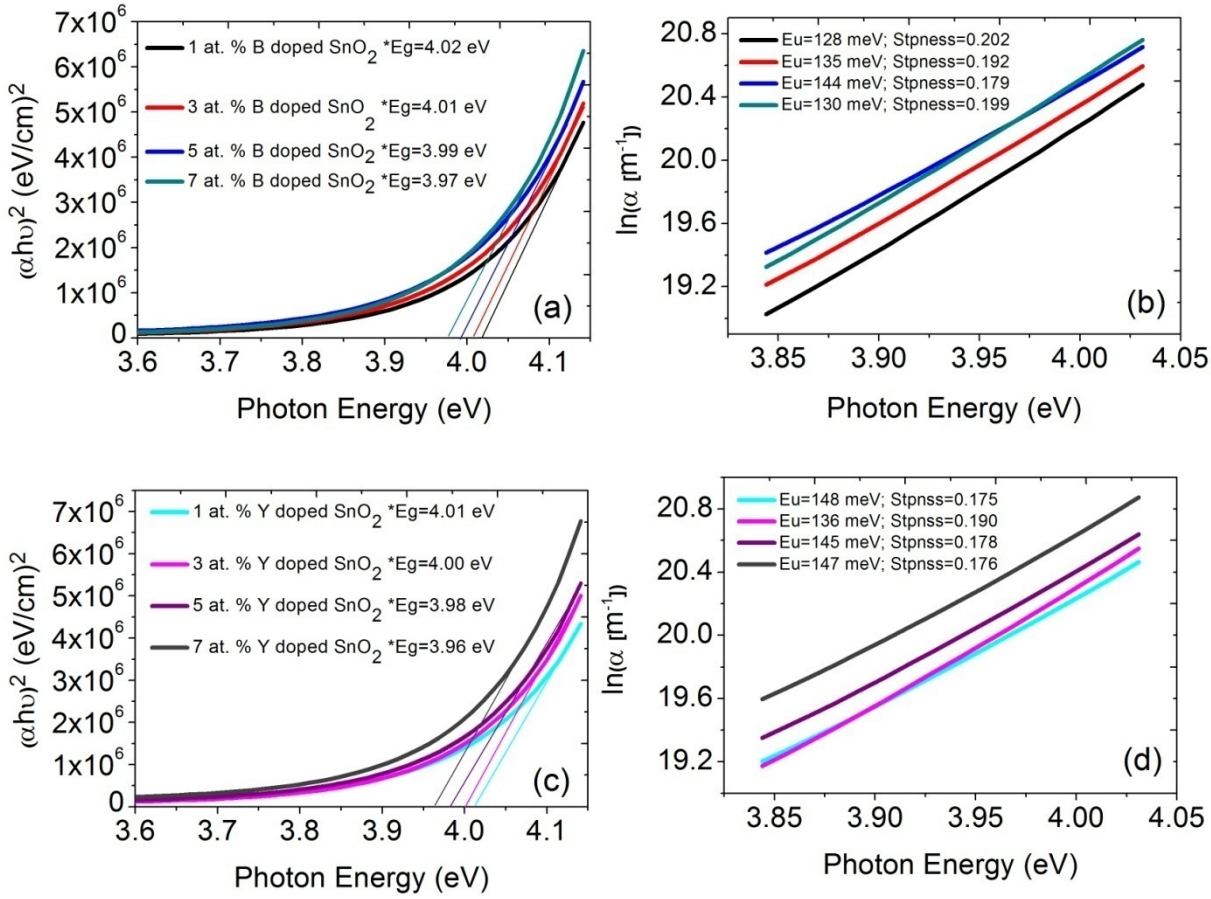

Fig. 5. The variation of hv vs. $(\alpha hv)^2$ and hv vs. ln(α) for B and Y doped SnO_2 films

4. Conclusion

In the present paper, B and Y doped SnO_2 thin films were successfully produced by sol-gel spin coating method. Characteristic properties of the films were investigated depend on B and Y incorporations. From the XRD studies, in generally, SnO_2 crystalline occurs in the tetragonal rutile crystal nature, but there are also orthorhombic and cubic phases called as hetero-phase of SnO_2 in the atmospheric pressure. Both applying the B and Y doping, the peaks intensities of undoped samples have decreased continuously with increasing doping contents. In addition, the peak intensities of B doped samples are further than Y doped samples, which implies better crystalline of B doped films. The electrical properties of B and Y doped samples have studied by using four point probe method. The variation of sheet resistance with doping ratios measured. The

optical properties of thin films were investigated by UV-Vis spectrometer at the room temperature. From these measurements, refractive index (n) of the samples, extinction coefficient (k), band gab values and Urbach energy-steepness parameters of samples were calculated. It was observed that band gap values of both B and Y doped films were decreased with increasing doping concentration and a fluctuation was observed to the Urbach energy and steepness parameters of the samples. Consequently B and Y incorporation affected the SnO_2 crystal and B doping effect is more than Y doping.

Acknowledgments

This work was supported by Atatürk University Research Fund, Project Number 2012/283.

References

[1] Q. Mao, Z. Ji, L. Zhao,Phys. Status Solidi b **247**(2), 299 (2010).
[2] Z. Ji, L. Zhao, Z. He, Q. Zhou, C. Chen, Materials Letters **60**, 1387 (2006) -1389.
[3] E. Elangovan, S. A. Shivashankar, K. Ramamurthi, Journal of Crystal Growth **276**, 215 (2005).
[4] K.S. Kim, S.Y. Yoon, W.J. Lee, K.H. Kim, Surface and Coating Technology **138**, 229 (2001) .
[5] S. Chacko, N.S. Philip, K.G. Gophandran, P. Koshy, V.K. Vaidyan, Applied Surface Chemistry 254, 2179 (2008).
[6] E. Elangovan, M.P. Singh, K. Ramamurthi, Materials Science and Engineering B **113**, 143 (2004).
[7] A.V. Moholkar, S.M. Pawar, K.Y. Rajpure, P.S. Patil, C.H. Bhosale, Journal of Physics and Chemistry of Solids **68**, 1981 (2007).
[8] M. Batzill, U. Diebold, Progress in Surface Science **79**, 47 (2005).
[9] C.Kılıç, A. Zunger, Physical Review Letters **88**(9) (2002).
[10] P. Nunes, E. Fortunato, P. Tonello, F.B. Fernandes, P. Vilarinho, R. Martins, Vacuum **64**, 281–285 (2002).
[11] A.R., Babar, S.S. Shinde, A.V. Moholkar, C.H. Bhosale, J.H. Kim, K.Y. Rajpure, Journal of Alloys and Compounds **505**(2), 416 (2010).
[12] A.V. Moholkar, S.M Pawar, K.Y. Rajpure, S.N. Almari, P.S. Patil, C.H. Bhosale, Solar Energy Materials and Solar Cells **92**, 1439 (2008).
[13] Z. Ji, Z. He, Y. Song, K. Liu, Z.Z. Ye, Journal of Crystal Growth **259**, 282 (2003).
[14] J. Joseph, V. Mathew, and K. E. Abraham, Cryst. Res. Technol. **41**(10), 1020-1026 (2006).
[15] B. Zhang, Y. Tian, J.X. Zhang, W. Cai, Vacuum **85**, 986-989 (2011).
[16] S.A. Nasser, Thin Solid Films **342**, 47-51 (1999).
[17] H.V. Fajardo, E.Longo, L.F. D. Probst, A. Valentini, N. L. V. Carreno, M.R. Nunes, A.P. Maciel, E.R. Leite, Nanoscale Res Lett **3**, 194-199 (2008).
[18] S. Rembeza, E. Rembeza, E. Russkıh, N. Kosheleva, Sensors & Transducers Journal **110**(11), 71-77 (2009).
[19] F.E. Ghodsi, H. Absalan, Acta Physica Polonica A **118,** 659-664 (2010).
[20] P. Sagar, M. Kumar, R.M. Mehra, Materials Science-Poland **23**, 685-696 (2005).
[21] M.R. Roknabadi, M. Behdani, H. Arabshahi, N. Hodeini, International Review of Physics **12**, 153-157 (2009).
[22] S. Ilıcan, Y. Caglar, M. Caglar, J. Optoelectron. Adv. Mater. **10**, 2578 (2008).
[23] A.R. Shien, High-pressure phases in SnO_2 to 117 GPa. Physical Review B **73**, 014105 (2006).
[24] J. Haines, J.M. Legér, Physical Review B **55**(17), 1144 (1997).
[25] P.S. Patil, R.K. Kawar, S.B. Sadale, P.S. Chigare, Thin Solid Films **437**, 34 (2003).
[26] C. Agashe, R. C. Aiyer,.Int. J. Appl. Ceram. Technol. **5**(2), 181 (2008).
[27] B. Hariprakash, A. U. Mane, S. K. Martha, S. A. Gaffoor, S. A. Shivashankar, Electrochemical and Solid-State Letters, 7, A66-A69 (2004).
[28] J. Gao, C. Jiang, J. Ying, C. Wan, J Power Source **155**, 364 (2006).

[29] P. Scherrer, Math. Phys. Kl., 98-100 (1918).
[30] K. Ravichandran, G.Muruganantham, B.Sakthivel, Physica B **404**, 4299–4302 (2009).
[31] N. N. Greenwood, A. Earnsha, Chemistry of the Elements, Second Edition, Elseiver, Oxford, UK, 1997.
[32] R.L. Mishra, S.K. Mishra, S.G. Prakash, Journal of Ovonic Research **5**(4), 77 (2009).
[33] S. Aksoy, Y. Caglar, S. Ilıcan, M. Caglar, Optica Applicata **6**(1), 7-14 (2010).
[34] D. Dabajyoti, B. Ratnabali, Thin solid **films147**(3), 321 (1987).
[35] M. Fantini, I. Torriani, Thin Solid Films **138**(2), 255 (1986).
[36] K.Y. Rajpure, M.N. Kusumade, M.N. Neumann-Spallart, C.H. Bhosale, Materials Chemistry and Physics **64**, 184-188 (2000).
[37] H. Fujiwara, M. Kondo, Physica Review B **71**(7), 075109 (2005).
[38] D. Mergel, Z. Qiao, Journal of Physics D: Applied Physics **35**, 794-801 (2002).
[39] T. Serin, N. Serin, S. Karadeniz, H. Sarı, N. Tuğluoğlu, O. Pakma, Journal of Non-Crystalline Solids **352**, 209-215 (2006).
[40] J. Tauc, R. Grigorovici, A. Vancu, Phys Status Solidi (b) **15**, 627-637 (1966).
[41] A.R. Babar, S.S. Shinde, A.V. Moholkar, C.H. Bhosale, J.H. Kim, K.Y. Rajpure, Journal of Alloys and Compounds **509**, 3108 (2011).
[42] N.Muthukumarasamy, S.Jayakumar, M.D.Kannan, R.Balasundaraprabhu, Solar Energy, **83**, 522-526 (2009).
[43] F. Urbach, Phys. Rev. **92**, 1324 (1953).
[44] 49. G.D. Cody, T. Tiedje, B. Abeles, B. Brooks, Y. Goldstein: Phys. Rev. Lett. **47**, 1480 (1981).
[45] S.K. O'Leary, S. Zukotynski, J.M.J Perz: Non-Cryst. Solids **210**, 249 (1997).
[46] Y. Caglar, S. Ilican, M. Caglar, F. Yakuphanoglu: J. Sol-Gel Sci. Technol. **53**, 372-377 (2010).